THE OIL BOOM IN A CURRENT

by

RICHARD JOSEPH ROBBINS

S.B., Cornell University
(1968)

SUBMITTED IN PARTIAL FULFILLMENT OF THE

REQUIREMENTS FOR THE DEGREE OF

MASTER OF SCIENCE

at the

MASSACHUSETTS INSTITUTE OF TECHNOLOGY

June, 1970

Signature of Author _____
Department of Electrical Engineering, May 21, 1970

Certified by _____
Thesis Supervisor

Accepted by _____
Chairman, Departmental Committee on Graduate Students

THE OIL BOOM IN A CURRENT

by

RICHARD JOSEPH ROBBINS

Submitted to the Department of Electrical Engineering on May 21, 1970 in partial fulfillment of the requirements for the Degree of Master of Science.

ABSTRACT

The containment and subsequent collection of oil spilled on the open sea seems to be an advantageous approach to the problem of oil spills. This thesis has investigated the simplest realistic case, namely, a barrier holding oil in a steady current with no surface waves or wind. The oil boom was modelled by a vertical flat plate in the sediment flume of the Hydrodynamics Laboratory of the Department of Civil Engineering at Massachusetts Institute of Technology. The length scale was approximately 1/25 full scale. Force measurements were taken by means of LVDT force blocks. The operating holding capacities of a barrier in a current has been determined. Our results show that large volumes and long slicks can be expected for full barriers. The drag coefficient and the location of the drag force for barriers as modelled by a vertical flat plate has been determined for a range of operating conditions. The presence of oil can have a large effect on the forces and moments exerted on a boom.

THESIS SUPERVISOR: David P. Hoult

TITLE: Associate Professor of Mechanical Engineering

ACKNOWLEDGEMENTS

Work for this thesis was supported by the Federal Water Pollution Control Agency, Contract No. 15080 ESL and administered under Project No. DSR 71990 by the Division of Sponsored Research at Massachusetts Institute of Technology. Their support is gratefully acknowledged.

The author would like to thank Professor David P. Hoult of the Department of Mechanical Engineering for his supervision and guidance. The author would like to especially thank Professor Ralph H. Cross, III, of the Department of Civil Engineering for his guidance in doing the experimental work.

The help of Roy Milley of the Hydrodynamics Laboratory was appreciated. The responsibility for grammar and spelling goes to Janice Brunoff, whose help was much appreciated. The author would finally like to thank Rosmarie Geering for doing the typing.

TABLE OF CONTENTS

TITLE PAGE	1
ABSTRACT	2
ACKNOWLEDGEMENTS	3
TABLE OF CONTENTS	4
SYMBOLS USED	5
I. INTRODUCTION	7
II. APPARATUS	9
III. RESULTS	18
III.1. Slick Profile, Maximum Volume	18
III.2. Drag and Moment, Without Oil	28
III.3. Drag and Moment, With Oil	32
IV. CONCLUSION, RESULTS APPLIED TO FULL SCALE	41
REFERENCES	44
APPENDIX	45

SYMBOLS USED

A	Oil profile constant
b	Boom width (ft)
C_D	Drag coefficient = $D/\frac{1}{2}\rho dbU^2$
c_f	Skin friction coefficient = $\tau/\frac{1}{2}\rho U^2$
d	Boom draft (ft)
d_0	Depth of water in flume (ft)
d_B	Depth of water under boom (ft)
D	Drag (lb)
Δ	Specific gravity difference = $(\rho_w - \rho_0)/\rho_w$
ΔH_{Hg-H_2O}	Venturi head loss (ft of Hg)
F_1, F_{2A}, F_{2B}	Forces (lb)
F	Froude number = $U/(gd)^{1/2}$
F'	Densimetric Froude number = $U/(g\Delta d)^{1/2}$
g	Acceleration due to gravity (32 ft/sec^2)
h	Thickness of oil slick (ft)
h_s	Thickness change due to stagnation pressure (ft)
k_s	Sand grain size
ℓ	Slick length (ft)
L	Width of deployed boom (ft)
M	Moment about lower edge of boom (lb-ft)
μ, μ_w, μ_0	Viscosity, water viscosity, oil viscosity (lb/sec-ft)
Q	Volume flow rate (ft^3/sec)
R	Reynolds number = $Ud/\mu/\rho$
ρ, ρ_w, ρ_0	Density, density of water, density of oil (slugs/ft^3)

τ	Shear stress (lb/ft^2)
T	Tension force (lb)
θ, ϕ	Angles
U, U_0, U_B	Velocity, velocity of oil, velocity under barrier (ft/sec)
V	Volume per unit width (ft^3/ft)
x	Distance along slick from leading edge (ft)
z	Distance from lower edge of boom (ft)

I. INTRODUCTION

The problem of oil spilled on the open sea is currently of great concern, as is recently attested to by the Santa Barbara spill. At present there are no effective ways of attacking the problem. The most advantageous approach to controlling an oil spill seems to be its containment and subsequent collection. One method of containment involves surrounding the oil spill with a floating barrier, traditionally a log boom with a weighted canvas curtain.

This thesis was undertaken with the view of studying a barrier, in this case modelled by a vertical flat plate, as it interacted with a steady current and oil. Wave action was not investigated in this study. The problem of a boom containing oil in a steady current is the simplest realistic case to study. Water current with no wave action is a condition that might be found in rivers, in a calm sea, or when a barrier is towed through a calm sea. It is also part of the total situation with waves and wind present.

The design of an effective barrier must involve investigation of capacity, leakage, forces, and stability. A barrier containing oil in a steady current is completely specified, when the oil profile, forces, and moments are determined. The profile of an oil slick, as related to barrier draft and water speed, contains information about the volume of oil, the slick length, and when leakage will occur. The results of investigating slick profile is presented in Section III.1.

The required strength and construction of a barrier in a steady current is dependent on the forces exerted on it. For a stably

deployed boom, there exists a balance of forces and moments between the mooring system (cable tensions and floatation) and the forces due to the current and oil held. Results of investigating drag force and moment for a boom containing oil are presented in Sections III.2 and III.3.

The experimental work for this thesis was done on a scale model. A barrier containing oil in a current was modelled by a vertical flat plate in a flume. The length scale was about 1/25 full scale. Both high and low viscosity oils were used. A discussion of the apparatus is presented in Section II; scale model results as applied to full scale is presented in Section IV.

II. APPARATUS

The work for this thesis was performed in the sediment flume in the Hydrodynamics Laboratory of the Department of Civil Engineering at the Massachusetts Institute of Technology. The flat plate barrier model was suspended from a steel frame over the flume. The plate was connected to force blocks by thin steel wire. Associated electronics processed the force block outputs to give drag and moment.

The sediment flume of the Hydrodynamics Laboratory has a self-contained closed circulation system with an adjustable rate of flow. The flume has a fixed horizontal bed of width 30", an overall depth of 15", and a length of 40'. The flume has glass side walls. Figure 1 is a sketch of the flume. The flume is equipped with a venturi constriction and two pressure take-off points to a U-tube mercury monometer. For full velocity there is a maximum pressure head loss at the venturi of 1.5 feet; the conversion formula for head loss to volume flow rate is given in equation (1).

$$Q = 1.387(\Delta H_{Hg-H_2O})^{1/2} \qquad (1)$$

The accuracy using this formula for velocity determination is dependent on the operating conditions. The greatest source of errors is not equation (1) but the boundary effects of the flume side walls and bottom. The total accuracy for the experimental conditions of the determined velocity is around 5%.

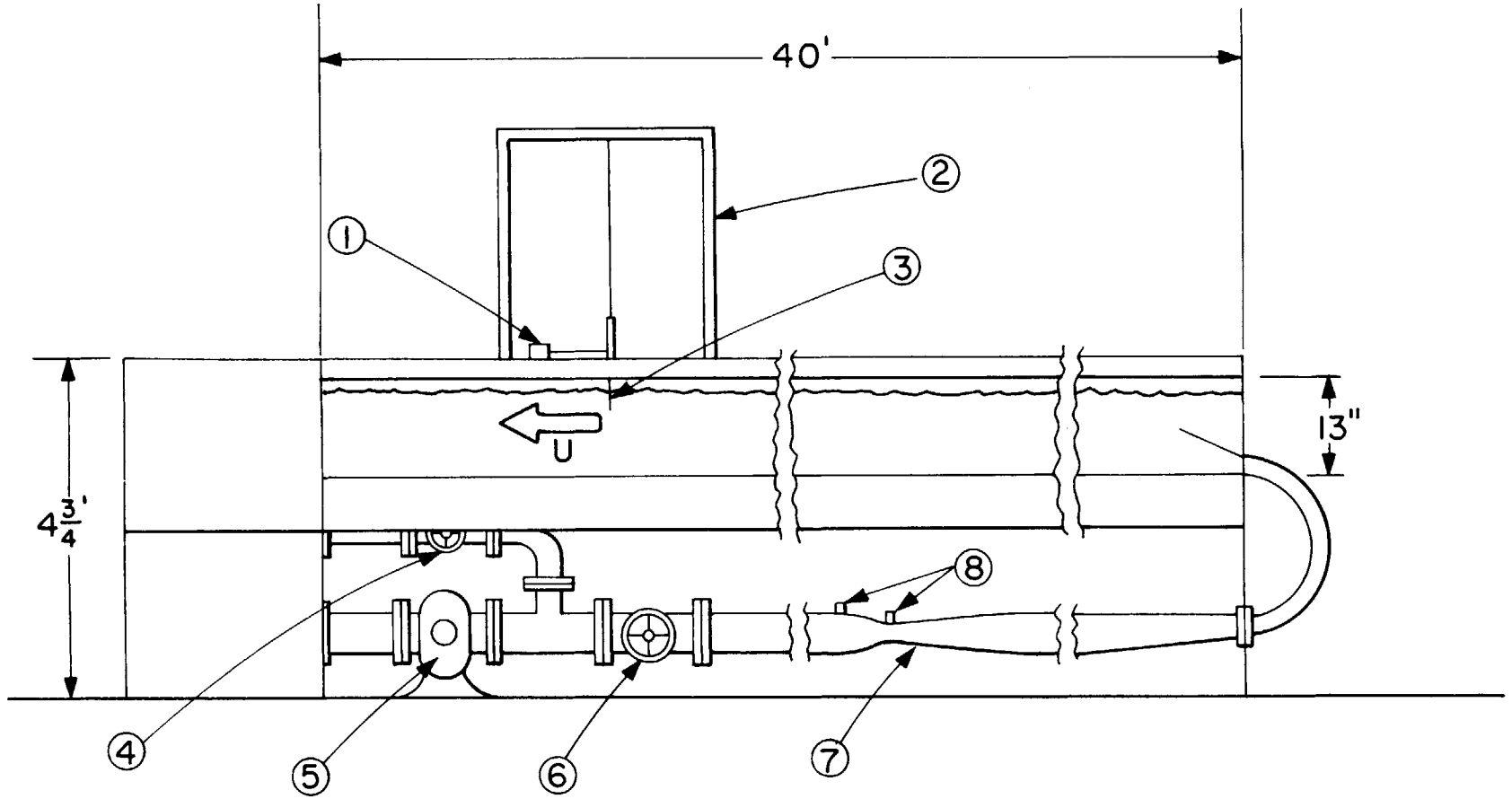

① LVDT force block
② Steel angle frame
③ Flat plate
④ By-pass valve
⑤ Pump
⑥ Main flow valve
⑦ Venturi constriction
⑧ Pressure take-offs

Figure 1. Sketch of flume

The vertical flat plate used in the boom model is suspended on wires from a rigid frame sitting on the sediment flume. The frame measures 3 1/2' by 3 1/2' by 3' and is made of steel angle pieces. The flat plate (both 1/8" aluminum and .030" steel were used) is connected to a 5/8" diameter aluminum tube frame which is suspended by 2 1/2' long aluminum wires. LVDT force blocks are connected in tension to the aluminum tube frame by thin flexible steel wire. One LVDT was connected 0.8' up from the lower edge of the barrier in the center of the flume channel. Two LVDT's were connected 0.4' up from the lower edge of the barrier 1 1/2" from each side. Two LVDT's were used at this level to keep the plate perpendicular to the current. These two sets of force measurements (three LVDT's) give the force couple from which moments and drag is calculated. The apparatus is sketched in Figure 2.

Linear Variable Differential Transformer force blocks consist of a set of coils and a core piece able to move only in an axial direction restrained by a spring. The force blocks used and the associated electronics had an output of $\pm$ 10 volts DC for a maximum force input of $\pm$1.0 pound and deflection of .030". The force blocks used were manufactured by Schaevitz Engineering.

In order to get drag and moment from the force measurements, equations (2) and (3) are used. These equations are derived from the free-body diagram of Figure 3 for the condition of zero deflection, no horizontal force supplied by the vertical wire supports, and no moments supplied by the wire connections to the force blocks. F_1 is the DC voltage derived from the LVDT located 0.8' from the lower edge, and

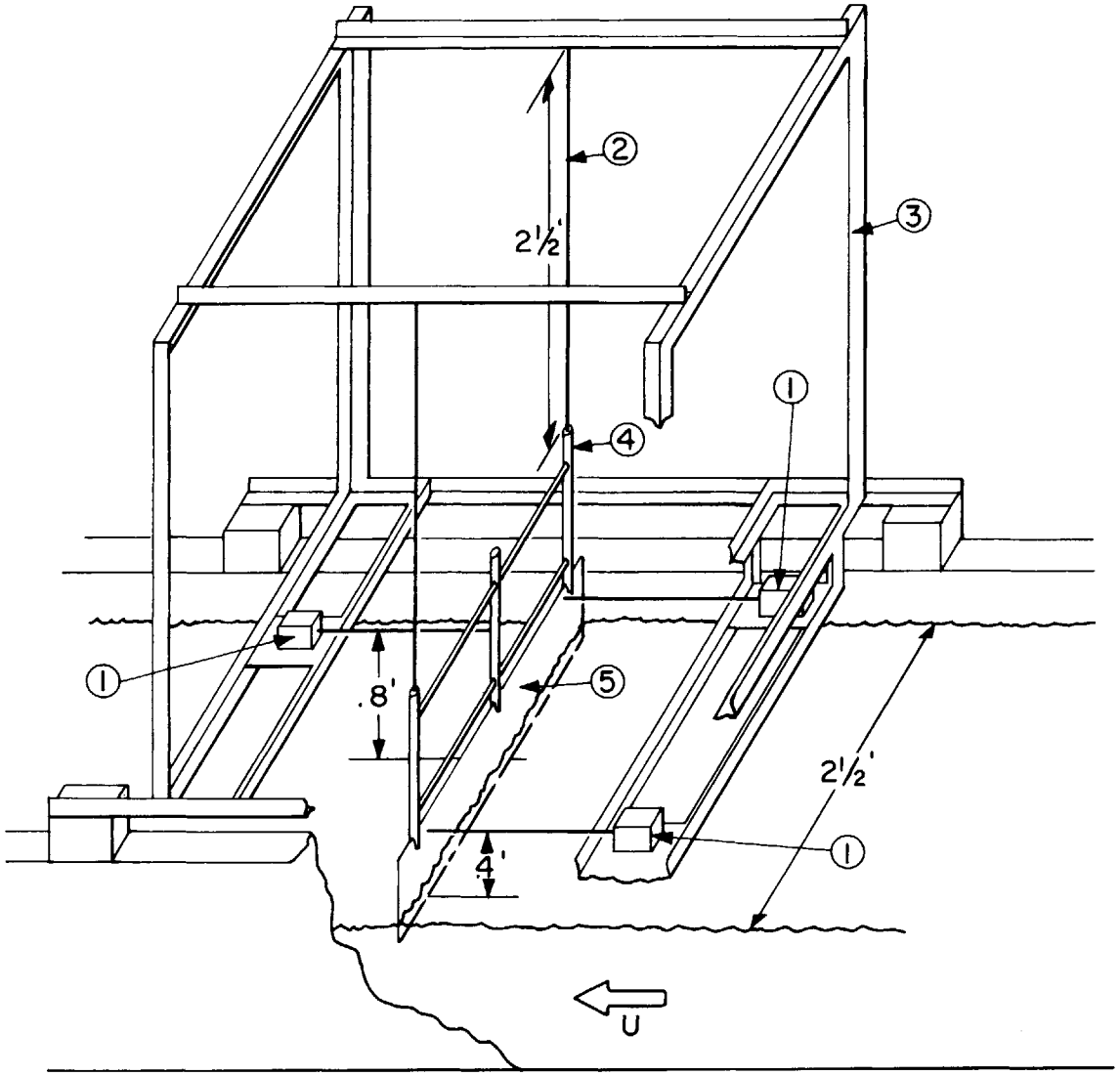

① LVDT force blocks ③ Steel angle frame ⑤ Flat plate
② Aluminum wire ④ Aluminum tube frame

Figure 2. Sketch of flat plate mounted in flume.

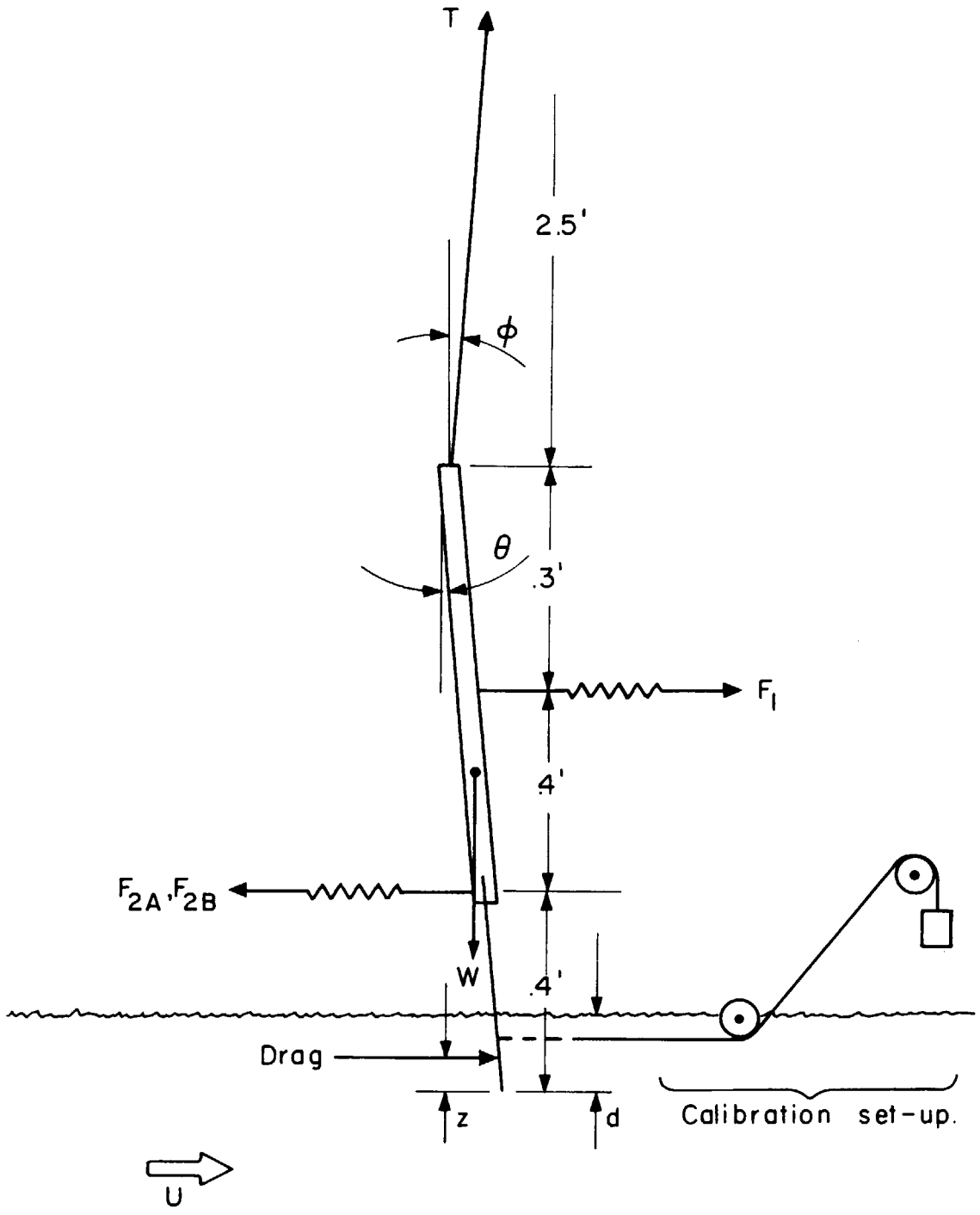

Figure 3. Free body diagram for plate and frame.

F_{2A} amd F_{2B} are the voltages from the LVDT's located 0.4' from the lower edge (positive voltage for tension); D_v and M_v are the drag and moment in terms of voltage.

$$D_v = (F_{2A} + F_{2B}) - F_1 \tag{2}$$

$$10M_v = 4(F_{2A} + F_{2B}) - 8F_1 \tag{3}$$

These equations were implimented by a Philbrick-Nixus RP-4 operational manifold consisting of five operational amplifiers (see Appendix for circuit diagram). The readout was done by a Honeywell digital voltmeter and rotary selector switch.

When equations (2) and (3) were implimented with the operational manifold, the voltage representing drag was within a few percent of the predicted value but that for moment had a large error. The reason for this is to get the moment voltage two numbers of equal order are subtracted and their difference amplified; therefore, a small error in alignment, the $\sin\theta$ times the weight error, horizontal forces supported by the vertical wires, or a moment carried by the connections to the force blocks can have a large effect on the moment measured. This situation is outlined in the free-body diagram of Figure 3.

Since the measurement of drag and moment and not necessarily an optimal piece of equipment was desired, equations (2) and (3) were approximately implimented and with the alignment set, the gains of the force blocks were adjusted so D_v and M_v instead of F_1, F_{2A}, and F_{2B} were the proper values when the plate was pulled at various distances up from the lower edge with various weights. This allowed the alignment

errors not to be important as long as they were reproducible.

This scheme worked well enough for small changes in the position of the acting drag (either water current of dead weight pull). M_v but not D_v had a slight dependence on z for constant applied drag and moment. Gains were adjusted so D_v and M_v were correct for the 50% of the draft position and all readings were corrected via a calibration (usually less than 5%). Figure 4 is a typical calibration chart. Calibrations were taken everytime a series of runs were made.

With the above calibration procedure the errors in the readings, after being corrected from the calibration chart, consisted of the reproducibility error and a zero shift error. The reproducibility error included drift in the electronics, friction in the calibrating pulleys, and alignment error in the dead weight calibration. The zero shift error occurred because of the construction of the LVDT's and consisted of failure of the zero force reading to duplicate before and after a run. This zero shift error did not cause the calibration to change as long as the zero force reading was subtracted off the reading; the LVDT's were found to be linear to better than 1%. These errors are plotted in Figure 5.

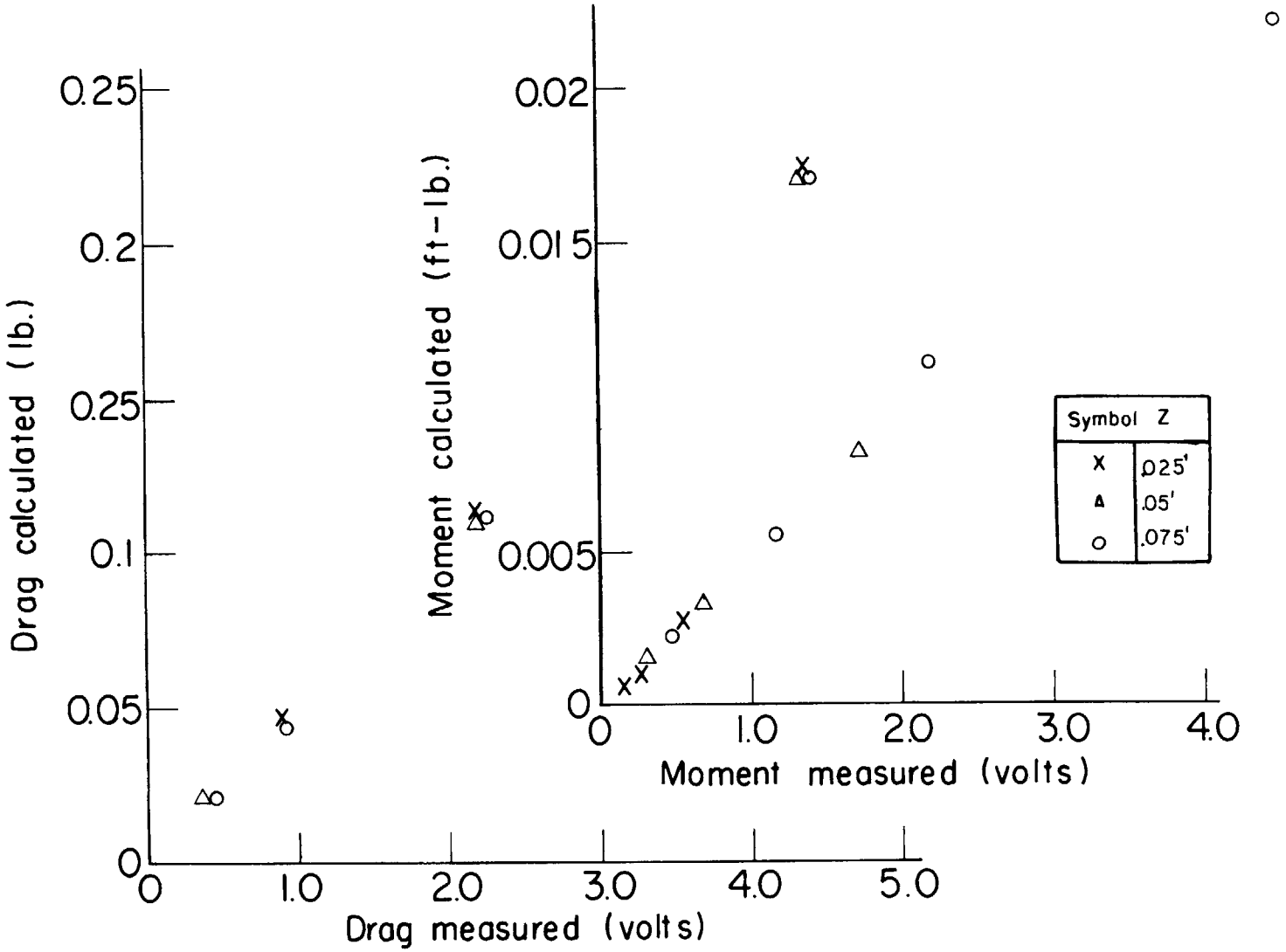

Figure 4. Apparatus calibration chart.

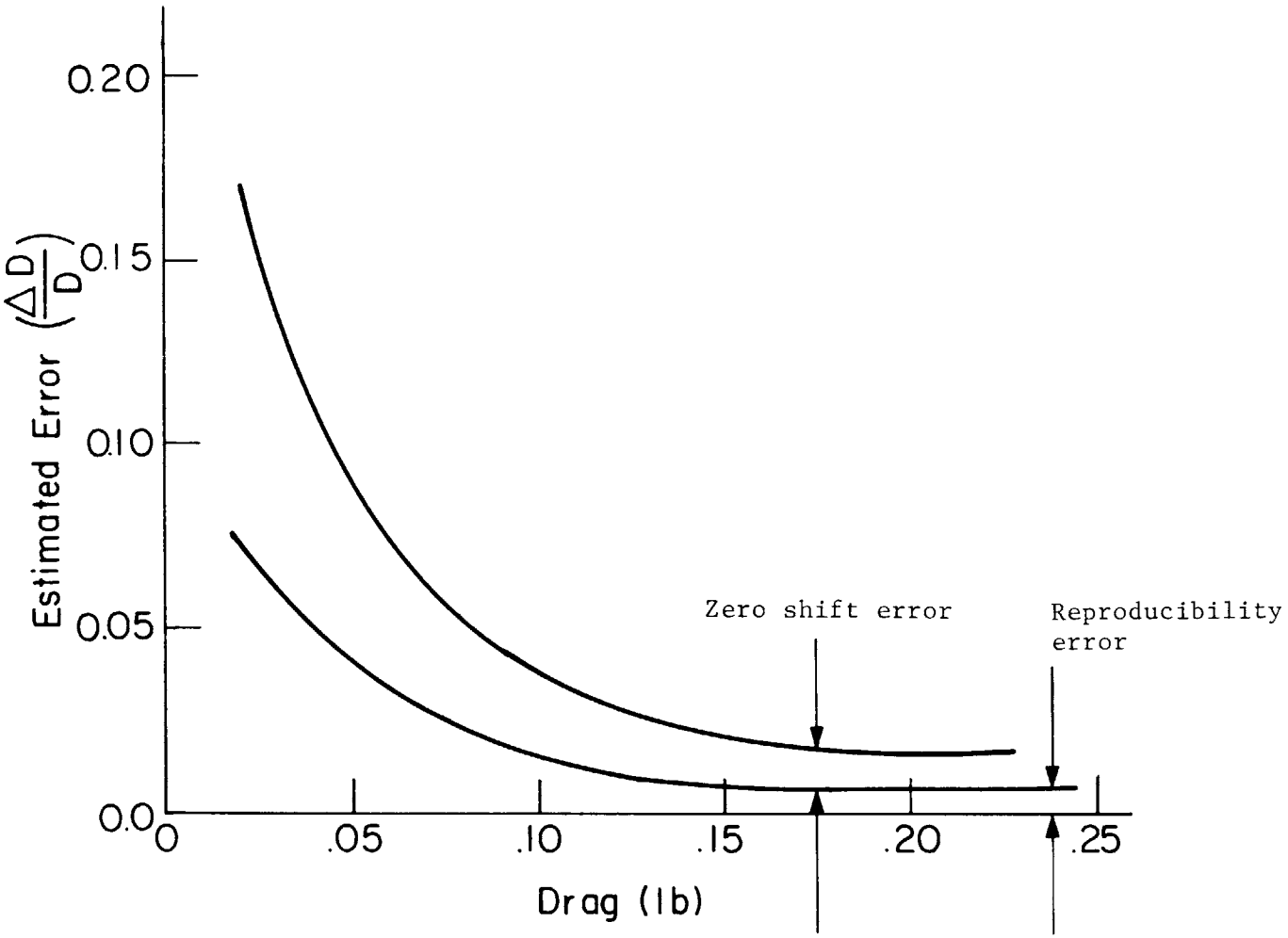

Figure 5. Estimated error of measured drag versus drag.

III. RESULTS

III.1. Slick Profile, Maximum Volume

When oil is held against a barrier by a steady current without surface waves, several things can be observed: a) the slick becomes progressively thicker moving from the leading edge to the barrier; b) within several boom drafts of the barrier the thickness decreases slightly; c) the upper surface of the slick is smooth while the lower surface can have waves; d) the interfacial waves tend to grow from the leading edge; e) there are circulatory motions in the slick, the lower surface moving with the current and the upper surface moving back; f) leakage occurs when the crest of the interfacial waves are carried under the barrier. This draw down phenomenon is sketched in Figure 6.

The current under the oil slick can be expected to exert a turbulent stress on the oil interface. This stress is partially balanced by motions in the oil and gradients in the oil thickness. If it is assumed that the shear force exerts no vertical component, then the oil is vertically in hydrostatic equilibrium, Δh of the slick is above the mean water level and $(1 - \Delta)h$ is below (Δ being the difference in specific gravities, typically around 1/10). A balance of forces in the horizontal direction yields equation (4)[1]

$$\frac{\partial}{\partial x} \int_{-(1-\Delta)h}^{\Delta h} \rho_0 U_0^2 dz + \rho_w g \Delta h \frac{dh}{dx} + \tau = 0 \quad . \tag{4}$$

The first term in equation (4) is the rate of change of momentum in the oil volume, the second is the hydrostatic force, and the third

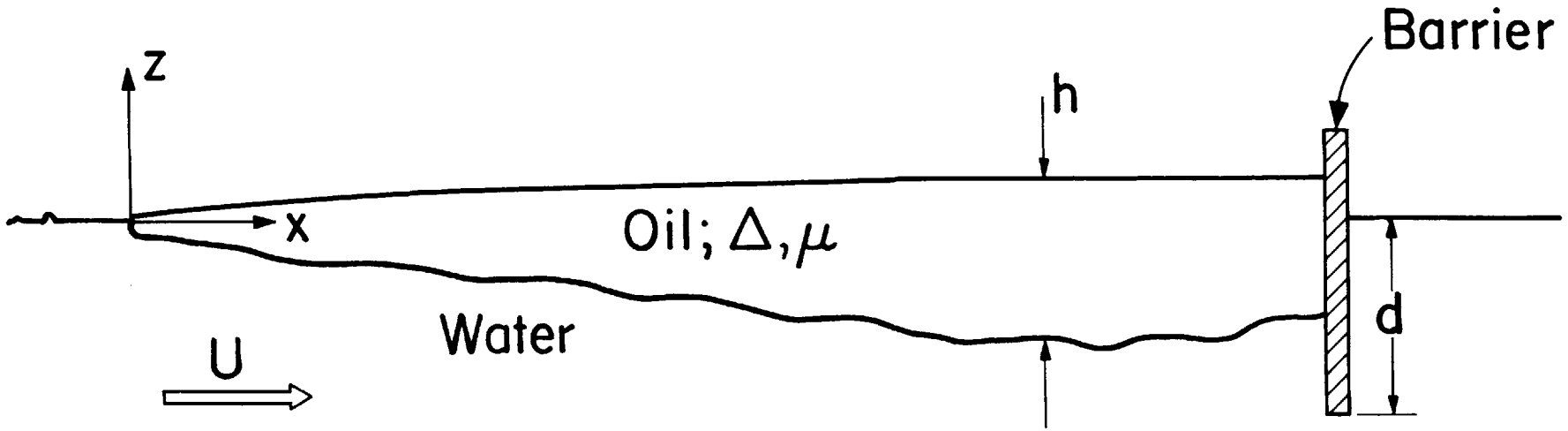

Figure 6. Sketch of draw down phenomenon

term is the turbulent stress. Continuity of mass implies equation (5)

$$\int_{-(1-\Delta)h}^{\Delta h} \rho_0 U_0 dz = 0 \quad . \tag{5}$$

It was not attempted to measure the velocity in the oil or the shear stress at the interface; runs consisted of measuring the thickness of the slick as a function of position along the slick for a certain current speed, oil volume, and boom draft. Maximum volumes held by the vertical flat plate were also measured.

Because of the dimensions of a slick, it is reasonable to assume that the profile of the slick far from the barrier (10d away, about 10% of the slick length) is independent of the barrier geometry. Thus h for the far-field can only be a function of x (the distance from the leading edge), $g\Delta$ (Δ effecting only buoyancy), U, ρ, and possibly the viscosity of the oil and water[2]. The possible nondimensional combinations of these variables are $xg\Delta/U^2$, $Ux/\mu_0/\rho_0$, $Ux/\mu_w/\rho_w$, and μ_0/μ_w. The first is a Froude number, the second and third are Reynolds numbers based on oil and water respectively, and the last is a viscosity ratio. Data for oil profiles for soybean oil ($\mu = 7.5 \times 10^{-2}$ lb/ft-sec, $\Delta = .077$) and #2 fuel oil ($\mu = 3.8 \times 10^{-3}$ lb/ft-sec, $\Delta = .138$) are plotted in terms of Froude numbers based on x and h in Figure 7. In this figure the effects of Reynolds number over the range of x and h are assumed to be small. Oil slick profile data was taken through the glass walls of the flume. This method is accurate to about 10%.

The data for #2 fuel oil is fitted quite closely with the line given in equation (6),

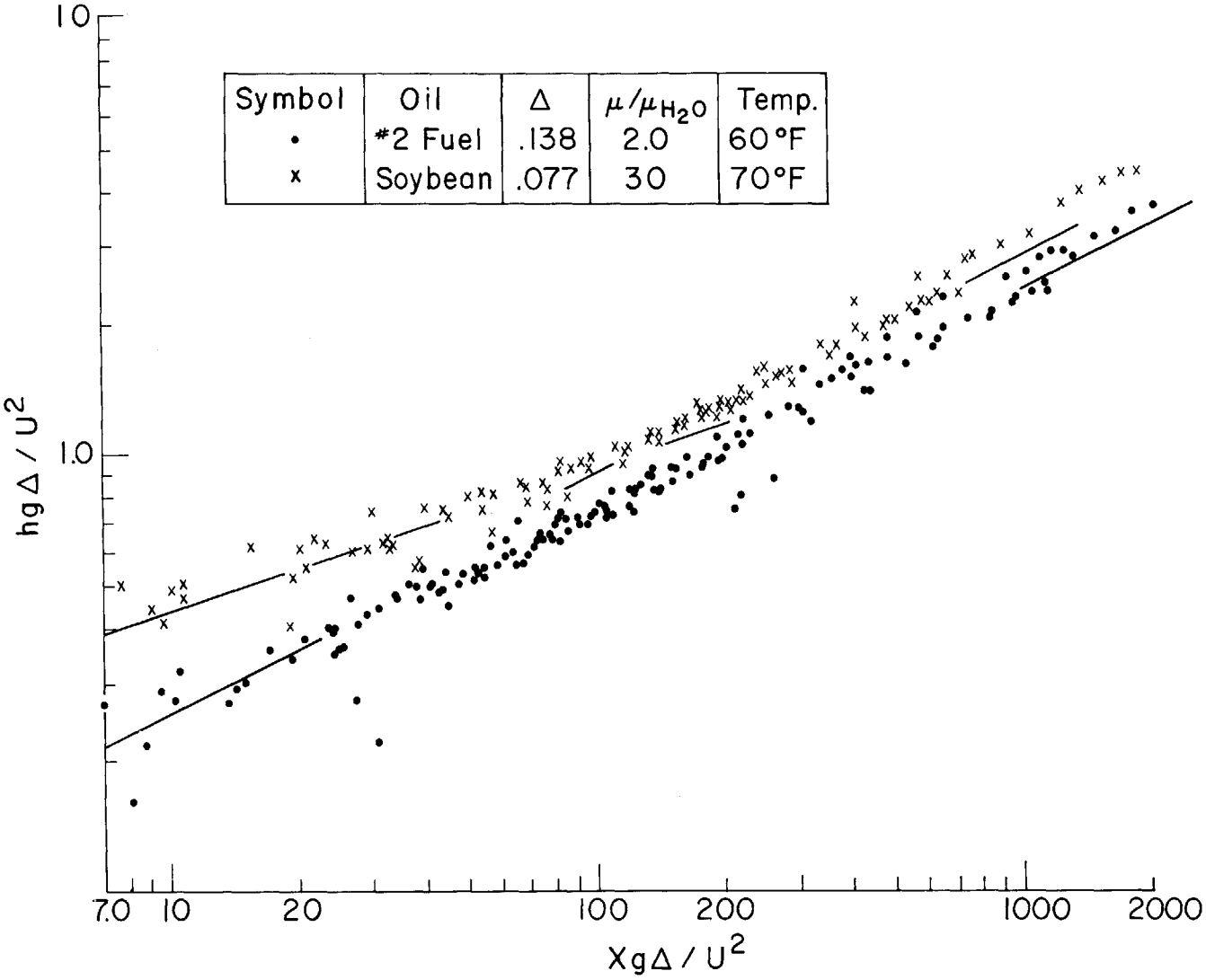

Figure 7. Non-dimensional oil thickness, $hg\Delta/U^2$ versus non-dimensional distance from the leading edge of the slick, $xg\Delta/U^2$

$$\left(\frac{hg\Delta}{U^2}\right) = (.072)\left(\frac{xg\Delta}{U^2}\right)^{1/2} \quad . \tag{6}$$

The data for soybean oil is best fitted by two lines; for $xg\Delta/U^2$ less than 120, equation (7) applies and for $xg\Delta/U^2$ greater than 120, equation (8) applies.

$$\left(\frac{hg\Delta}{U^2}\right) = (0.20)\left(\frac{xg\Delta}{U^2}\right)^{.36} \tag{7}$$

$$\left(\frac{hg\Delta}{U^2}\right) = (.090)\left(\frac{xg\Delta}{U^2}\right)^{1/2} \tag{8}$$

The profile data for equations (6), (7), and (8) did not include measurements near the leading edge or near the barrier. Because of the slight instability of the leading edge, careful data near the edge was difficult to acquire and no data was taken for x less than 10d (about 10% of the slick length). Within several boom drafts of the barrier the oil thickness decreases slightly. This near field behavior was not included in Figure 7 because it depends on d as well as on x, Δg, U, and ρ.

One reason that the oil thickness decreases in the near-field is because of the stagnation pressure of the water against the barrier. The stagnation pressure can be estimated to be approximately $\frac{1}{2}\rho U^2$. If hydrostatic pressure is assumed in the oil, the thickness change due to the stagnation pressure is given by equation (9),

$$h_s = \frac{1}{2} U^2/g\Delta = \frac{d}{2} F'^2 \quad . \tag{9}$$

Equation (9) gives a reasonable estimate of this near-field behavior. This behavior can be expected to scale with the densimetric Froude number.

Since most of the volume of oil for booms holding large volumes is away from the barrier and away from the leading edge, profile equations (6) and (8) can be integrated to get volumes. For maximum volumes the equations are integrated until h = d. The error caused by neglecting the near-field thickness change and by extending the $x^{1/2}$ behavior out to the leading edge is small. The maximum volume held by a boom is therefore approximately a function of the oil profile and the draft. The volume per unit width by a dimensional argument has the functional dependence as in equation (10),

$$V = d^2 f(U^2/d\Delta g) \quad . \tag{10}$$

Data for maximum dimensionless volume per unit width versus densimetric Froude number is plotted in Figure 8. The slopes for the initial parts of this plot agree with the slopes predicted by integrating equations (6) and (8).

The presence of a critical densimetric Froude number, above which no oil is held, can be seen in Figure 8. This result can be expected because of the presence of interfacial waves. When interfacial waves are present it is not valid to say that leakage occurs when h = d. For densimetric Froude numbers much less than F'_{crit} leakage occurs when the oil thickness is greater than the boom draft; for densimetric Froude numbers close to F'_{crit} leakage occurs when the oil thickness plus the wave height is approximately the boom draft.

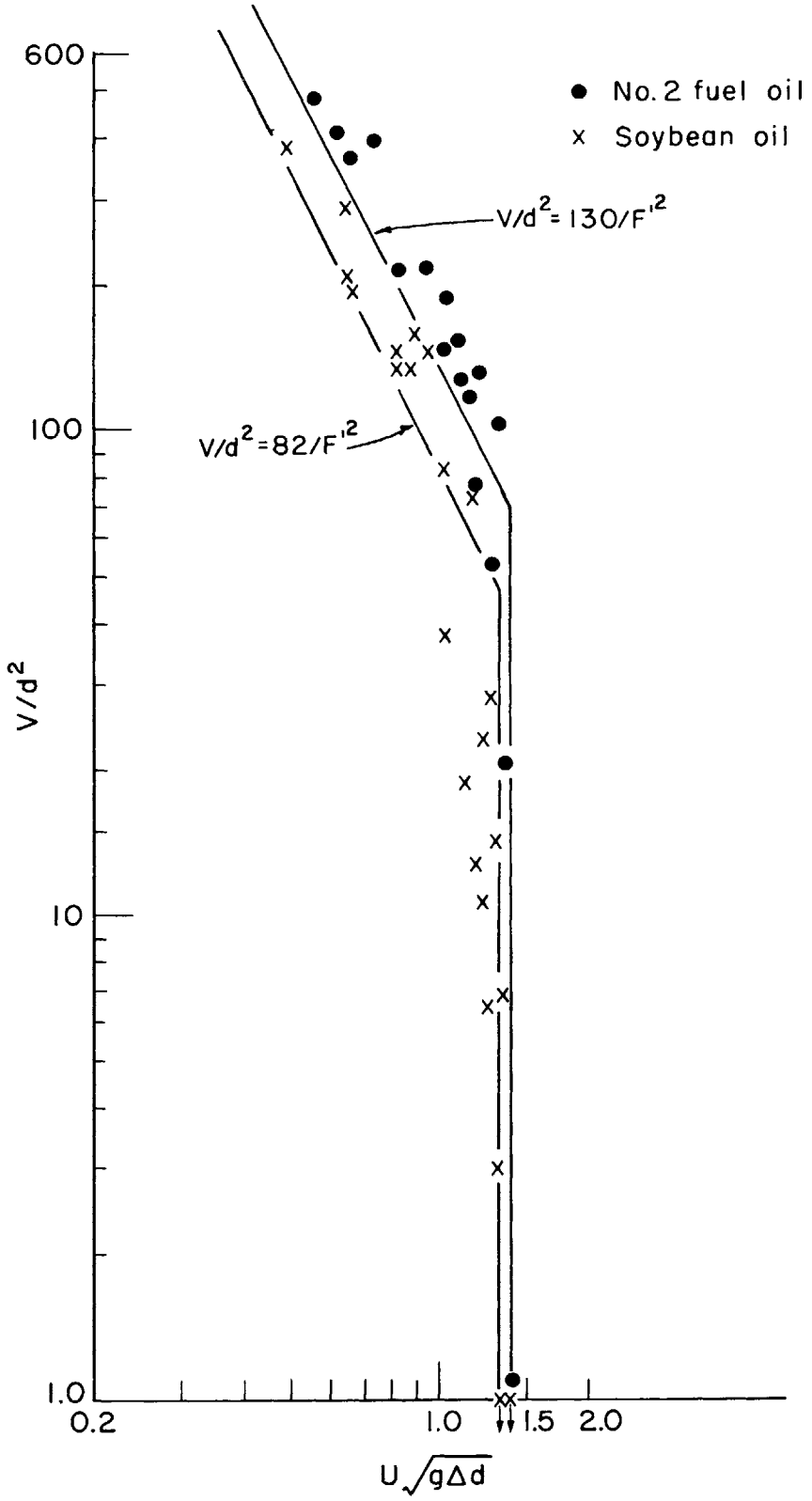

Figure 8. Non dimensional oil volume held, V/d^2, versus densimetric Froude number, $U\sqrt{g\Delta d}$

Data for dimensionless volume versus densimetric Froude number for scale model results show that for soybean oil $F'_{crit} = 1.31$ and for #2 fuel oil $F'_{crit} = 1.39$. It is not clear how this result can be predicted from theory or how it will scale to the prototype case.

Insight into how profile results and volume results (away from F'_{crit}) theoretically scale to the prototype case can be gained by comparing the turbulent stress on the oil slick and results from sand-roughened flat plates.

In order to determine the importance of shear stress in an oil slick, the terms of equation (4), the horizontal force balance, can be examined with an order of magnitude approach. Typical values for the variables in equation (4) are as follows: 1) oil velocity, U_0, about 0.1 ft/sec (as compared with U about 0.6 ft/sec), 2) slick thickness at the barrier, h_0, about 0.1 ft, 3) slick length, x_0, about 10 ft and 4) Δ about 1/10. The term dh/dx is approximately h_0/h_x. If a triangular distribution of oil velocity is assumed, the ratio of the change of momentum term to the pressure gradient term can be determined as in equation (11),

$$\frac{\rho g \Delta h \frac{dh}{dx}}{\frac{\partial}{\partial x}\int_{-(1-\Delta)h}^{\Delta h} \rho_0 U_0^2 dz} \approx \frac{\rho g \Delta h \frac{h_0}{x_0}}{\frac{(1-\Delta)\rho U_0^2 h}{2x_0}} \approx \frac{g\Delta h_0}{\frac{(1-\Delta)U_0^2}{2}} \approx 70 \quad . \qquad (11)$$

It is therefore safe to assume that the important characteristics of a slick profile in the model are described by a balance of shear force and pressure gradient, the change of momentum term being at least an

order to magnitude smaller. It can be expected that this will also be true in the prototype.

When the force is equated to the pressure gradient term of equation (4), the slick profile equation can be used to find the coefficient of skin friction, as defined by equation (12),

$$C_f = \frac{\tau}{\frac{1}{2}\rho U^2} = \frac{\rho g \Delta h \frac{dh}{dx}}{\frac{1}{2}\rho U^2} \quad . \tag{12}$$

When h has a $x^{1/2}$ dependence, as was experimentally determined, h(dh/dx) is not a function of x. The terms h(dh/dx) from equations (6) and (8) are given in equations (13) and (14), respectively.

$$h \frac{dh}{dx} = \frac{1}{2} (.090)^2 (\frac{U^2}{g\Delta}) \tag{13}$$

$$h \frac{dh}{dx} = \frac{1}{2} (.072)^2 (\frac{U^2}{g\Delta}) \tag{14}$$

When equations (13) and (14) are plugged into equation (12), the coefficients of skin friction for soybean oil and #2 fuel oil work out to be 8.1×10^{-3} and 5.1×10^{-3}, respectively.

Results for sand-roughened flat plates show that for low enough Reynolds number (Reynolds number based on x, the distance along the plate, U, μ, and ρ in the water) the plate looks smooth, that is, the coefficient of local skin friction decreases as the boundary layer developes along the length of the plate. For a constant roughness ratio k_s/x (constant k_s/x means that traversing along the plate, increasing x, the sand grain size increases accordingly), there is a Reynolds number

above which the coefficient of skin friction is constant[3].

The analogy of the oil slick with the sand roughened plate can be made at several points: 1) for long slicks (i.e. high range of Reynolds number) the skin friction coefficient is a constant, 2) for the higher viscosity soybean oil and nearer the leading edge, the skin friction coefficient decreases approximately as $x^{-0.28}$, and 3) sand roughness increasing as x can be compared with wave heights increasing as x. With this analogy in mind, an equivalent sand roughness can be found for soybean oil using the constant skin friction coefficient of the $x^{1/2}$ results and a Reynolds number based on water at the point where the $x^{1/2}$ behavior begins to fit the data (i.e. $xg\Delta/U^2 = 120$). Typical data for this point are x = 6 ft and U = .35 ft/sec for a Reynolds number of 2.1×10^5. This Reynolds number and c_f for soybean oil of 8.1×10^{-3} determine a sand roughness of $k_s/x = 3 \times 10^2$ [Ref. 4]. For x = 6 ft this is a roughness height of about 1/4"; this roughness height is roughly the observed wave heights of the interfacial waves.

The analogy of sand roughness to the oil slick seems to be good. What is in question is the effect of oil viscosity on the Reynolds number. Regardless of how the correct Reynolds number is determined, in the prototype case, where the Reynolds number will be higher than in the model, the analogy to sand roughness implies a constant skin friction coefficient. This conclusion implies that profile results for the $x^{1/2}$ behavior scale as the Froude number with no Reynolds number dependence. Prototype profile behavior for soybean oil and #2 fuel oil can be expected to be described by equations (6) and (8),

respectively. Equation (7) holds only for the very beginning of the soybean slick in the prototype.

III.2. Drag and Moment, Without Oil

The steady-state drag and moment exerted on a vertical flat plate in a current (no oil present) can be considered a function of the Froude number, the Reynolds number, the aspect ratios, and in a flume, a function of the water depth, side walls and velocity profile. Runs consisted of measuring the drag and moment about the lower edge as a function of current speed for a certain boom draft, d, and depth of water under the boom, d_B. From this the drag coefficient and the location of the drag from the lower edge, z/d were plotted versus Froude number, $U/(gd)^{1/2}$, for constant d/d_B.

It could be expected that if the Reynolds number is high enough, the main effects would be independent of viscosity. Reported results for both flat plates and disks normal to the flow and completely emersed in the flow (no free surface as in the barrier) show that the drag coefficient is constant for a Reynolds number above 10^3 and 10^2, respectively[5]. The experimental range of Reynolds numbers was from 10^3 to 10^4 (no oil), which is in the range to expect no Reynolds number dependence; no Reynolds number effects were seen in the data scatter.

The plate thickness used was 1/8" and .030" for a minimum draft to thickness ratio of about 8:1 and 32:1, respectively. Drafts for no oil runs were between .08' and .10', and drafts up to .20' were used for the no oil runs. No variation in data was noticed with this aspect ratio change. The width of the plate was 2.5' for a minimum width to

draft ratio of about 25:1. For this aspect ratio, C_D has approached the behavior of a plate of infinite length emersed normal to the flow[6].

The variation in results of measuring C_D and z/d versus Froude number for various drafts and water depths can be explained in terms of the variable d/d_B. The effects of water depth and draft on the moment and drag can be seen in Figure 9, C_D versus d/d_B for constant F, and Figure 10, z/d versus d/d_B for constant F. This blockage effect can be considered as being caused by the pressure head loss that in the prototype case ($d/d_B = 0$) would not be present. Considering only hydrostatic pressures, the head loss after the barrier would be proportional to the square of the velocity in the constriction, U_B, as in equation (16),

$$\rho g h \sim \frac{1}{2} \rho U_B^2 \quad . \tag{16}$$

Applying continuity of flow to get U_B in terms of U and forming the equality with the constant C_{D_0}, the drag coefficient is calculated in equation (17),

$$\begin{aligned} D &= (\tfrac{1}{2} \rho d b U_B^2) C_{D_0} = (\tfrac{1}{2} \rho d b U^2)(1 + d/d_B)^2 C_{D_0} \\ C_D &= (1 + d/d_B)^2 C_{D_0} \quad . \end{aligned} \tag{17}$$

The center of pressure for hydrostatic pressure is 1/3 up from the bottom; a simple calculation gives a location of the sum of the pressures on both sides of the barrier as in equation (18), where higher order terms in F have been dropped.

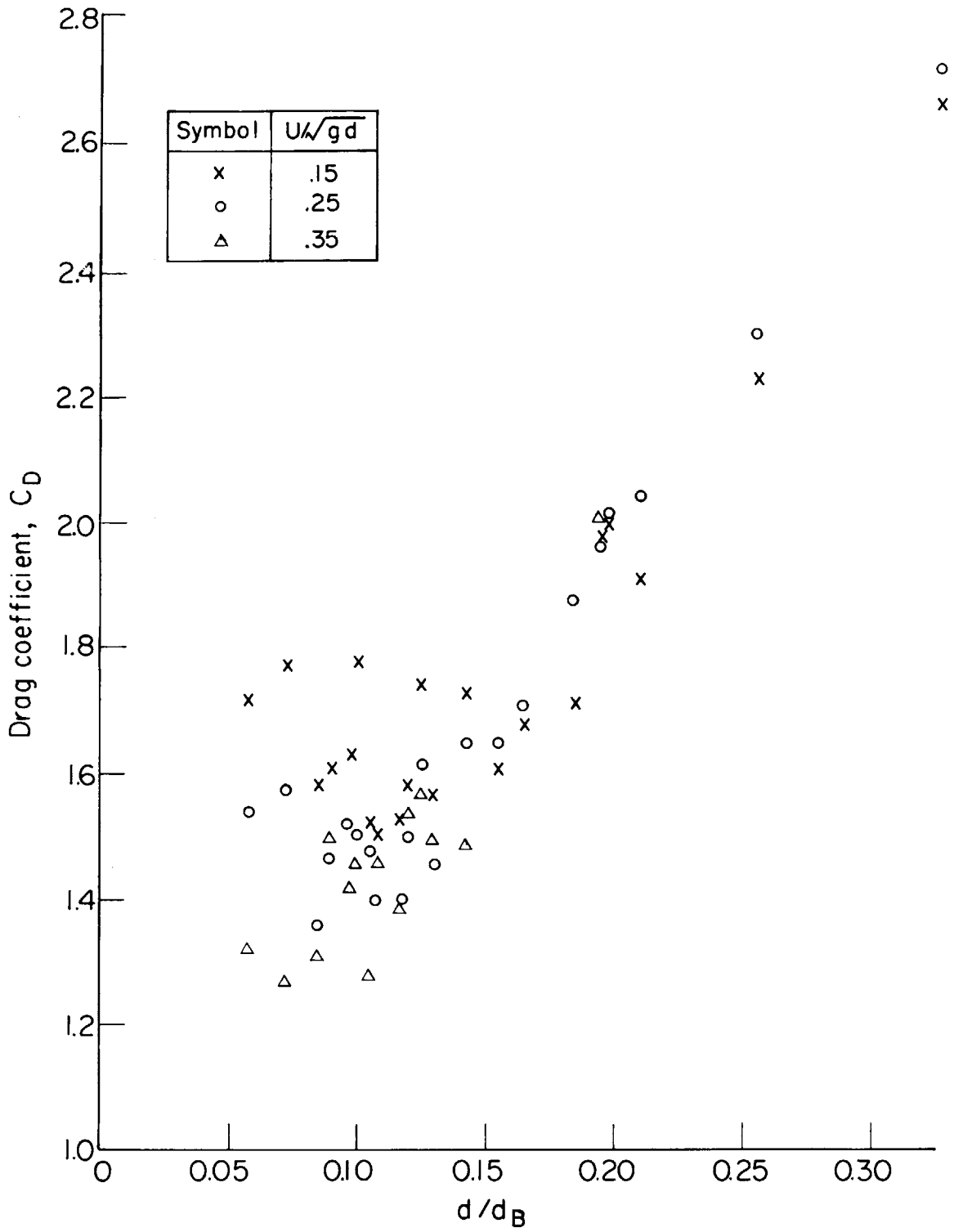

Figure 9. Drag coefficient versus blockage ration, d/d_B

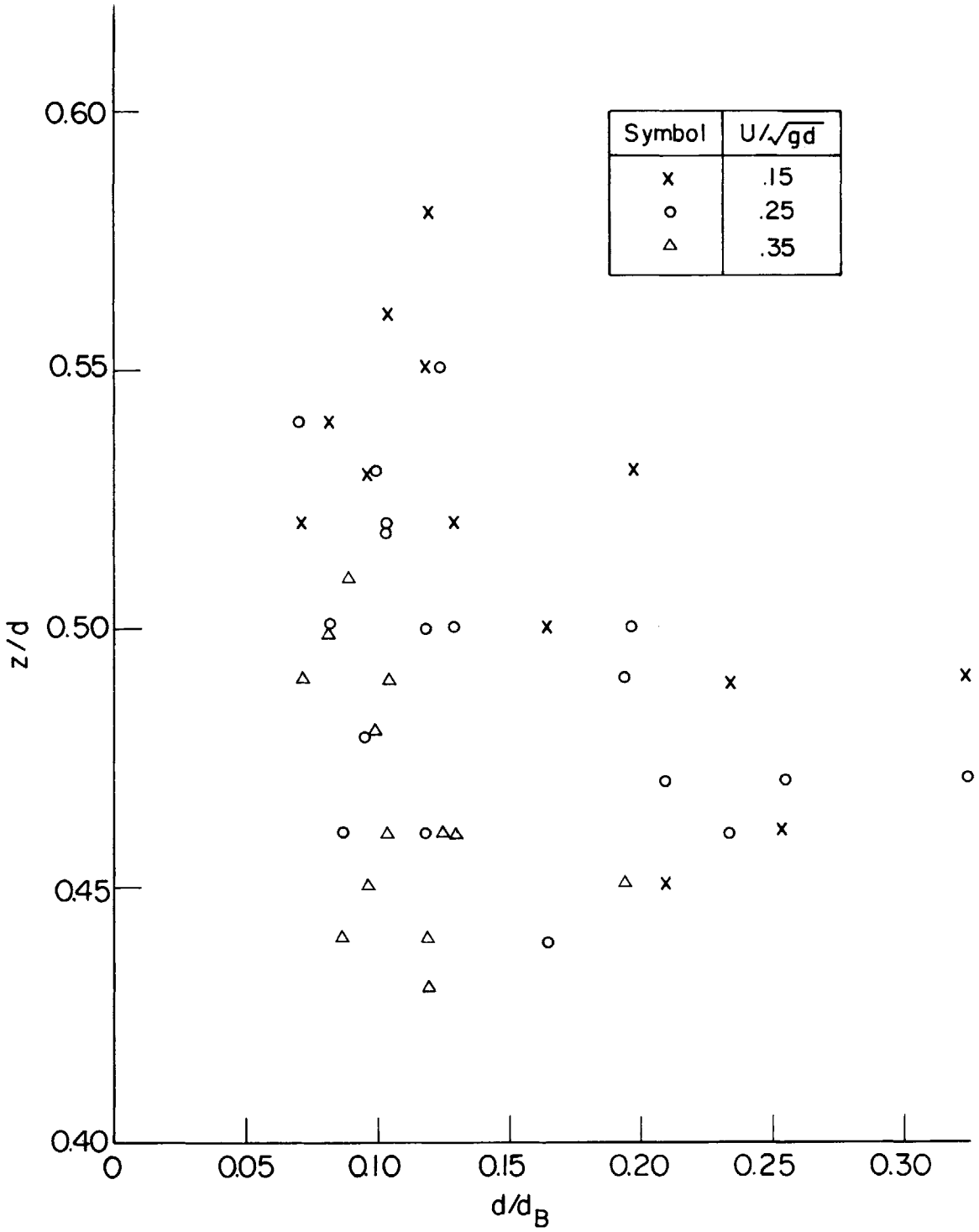

Figure 10. Location of drag from lower edge of boom, z/d, versus blockage ratio, d/d_B.

$$\frac{z}{d} = \left(\frac{1}{2} - \frac{1}{4} C_{D_0} (1 + d/d_B)^2 F^2\right) \qquad (18)$$

C_D and z/d for large d/d_B (greater than .15) follow this behavior of equations (17) and (18).

In the case of interest, a barrier in deep water (limit d/d_B goes to zero), it can be seen that for d/d_B between .15 and .07, depending on the Froude number, the asymptotic behavior has been approached. C_D and z/d versus Froude number are plotted in Figures 13 and 14 for the limit d/d_B goes to zero according to the d/d_B plots. Error bars for these figures were experimentally determined by the scatter in the data of the d/d_B for constant F plots at the point where the curve approaches its asymptotic behavior. This scatter is close to that predicted by the estimated error curve, Figure 5.

The drag and moment results for the no oil case scale as the Froude number, where the barrier is expected to behave like a flat plate emersed in a flow, namely, to have no Reynolds number dependence in the range of interest. For the draft to thickness ratio and width to draft ratio used the plate can be considered a good model of an infinitely long thin plate.

III.3. Drag and Moment, With Oil

The steady-state drag and moment exerted on a vertical flat plate in a current with various amounts of oil present can be considered to have the same functional dependence as in the no oil case but also a functional dependence on the difference in specific gravities, Δ, the amount of oil present, and the viscosity of the oil. Runs consisted of measuring the drag and moment about the lower edge of the plate for

a certain current, draft, and water depth, and gradually increasing the amount of oil from zero to full barrier and steady leakage.

The relative depth of oil next to the boom can be considered as the independent variable as opposed to the volume. This relative depth is a function of volume, densimetric Froude number, and viscosity (see Section III.1). The statics of the vertical forces in the slick show that the oil stands Δh above the water level and $(1 - \Delta)h$ below the water level, where h is the thickness of the slick. C_D and z/d are plotted in Figures 11 and 12 for constant Froude number, Δ, and viscosity as a function of $(1 - \Delta)h/d$. The variable $(1 - \Delta)h/d$ is zero for no oil and one for full barrier. For higher Froude numbers, the interfacial waves do not allow a barrier to become uniformly full. Full barriers for higher Froude number occur for $(1 - \Delta)h/d$ around .90.

With an oil slick present in front of the barrier in the flume, the cross-sectional area from which the velocity is calculated, knowing the volume flow rate, can change by up to 10% due to the blockage of the oil. The velocity used to calculate C_D and F was this velocity under the slick and not the velocity far upstream. This oil blockage is considered to be different from the no oil blockage by the barrier, where asymptotic behavior was reached around $d/d_B = .10$, because of the extent of the blockage (usually the slicks were artificially terminated at a distance 4' upstream). The experimental set up did not allow for much variation in d_B so the effects of oil blockage (asymptotic behavior of h/d_B) were not investigated. All oil runs were taken where the d/d_B dependence had reached asymptotic behavior. Using the velocity under the oil slick is reasonable; at most there

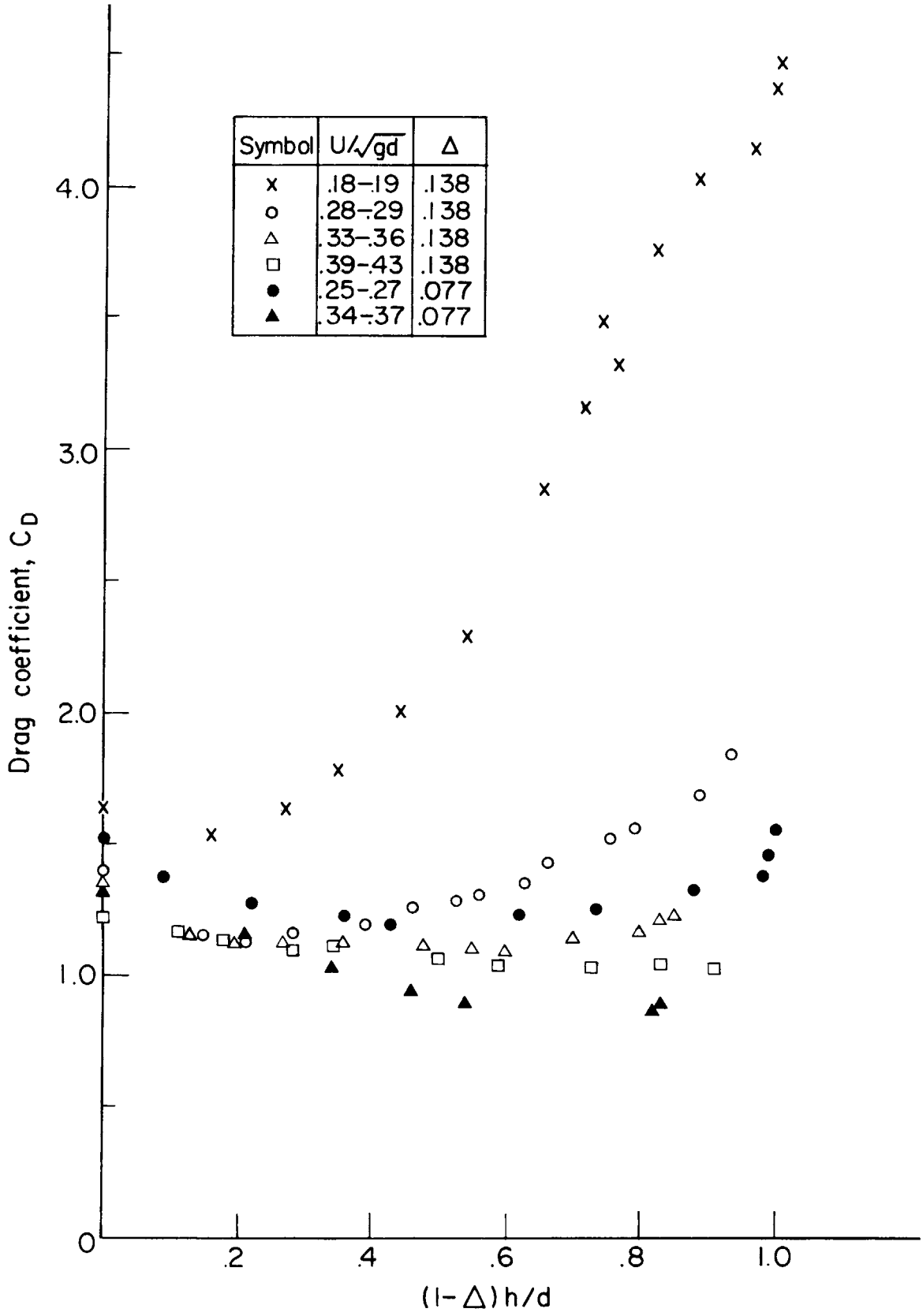

Figure 11. Drag coefficient versus relative oil depth, $(1-\Delta)h/d$.

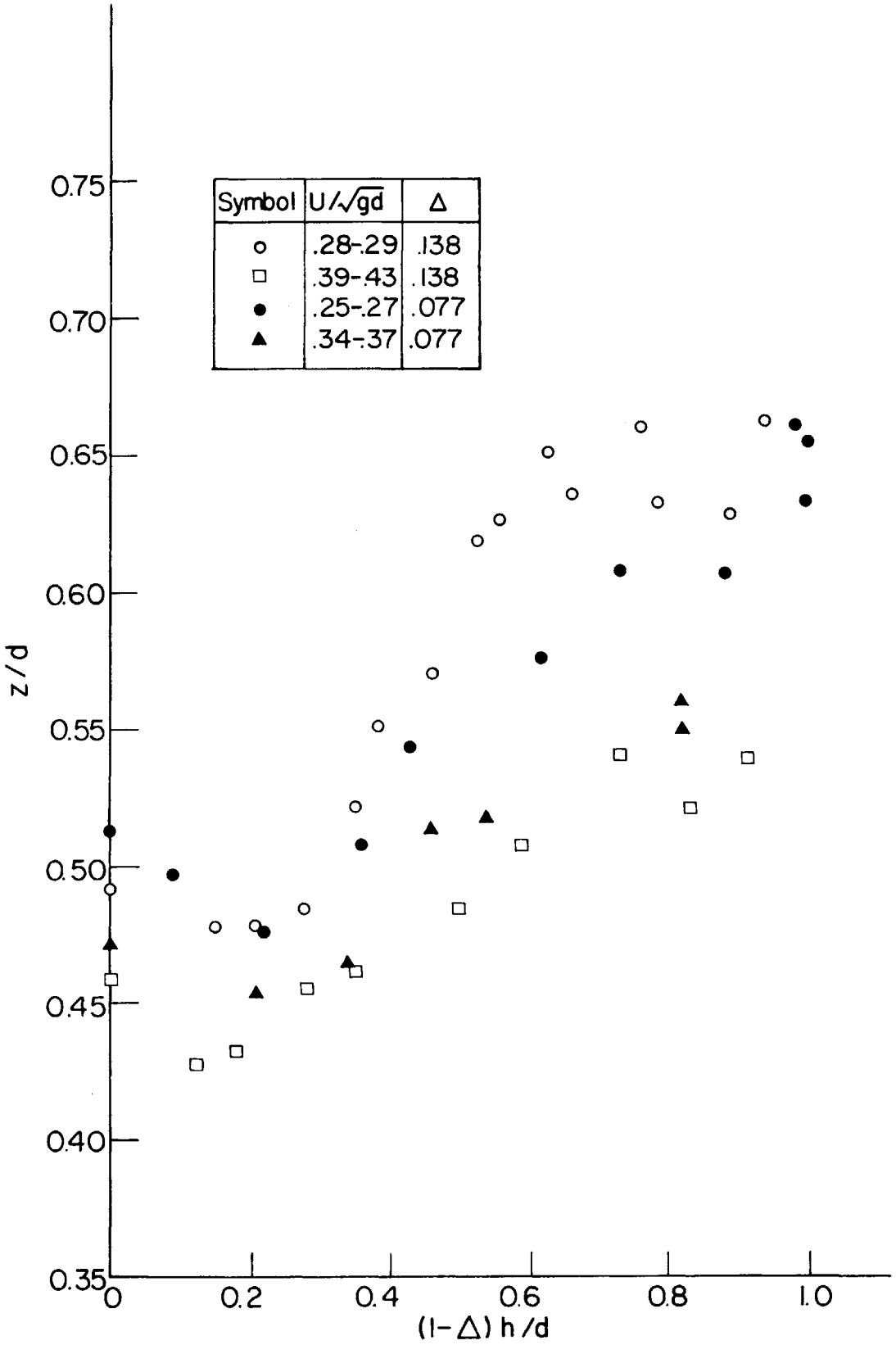

Figure 12. Location of drag force from lower edge of boom, z/d, versus relative oil depth, (1-Δ) h/d.

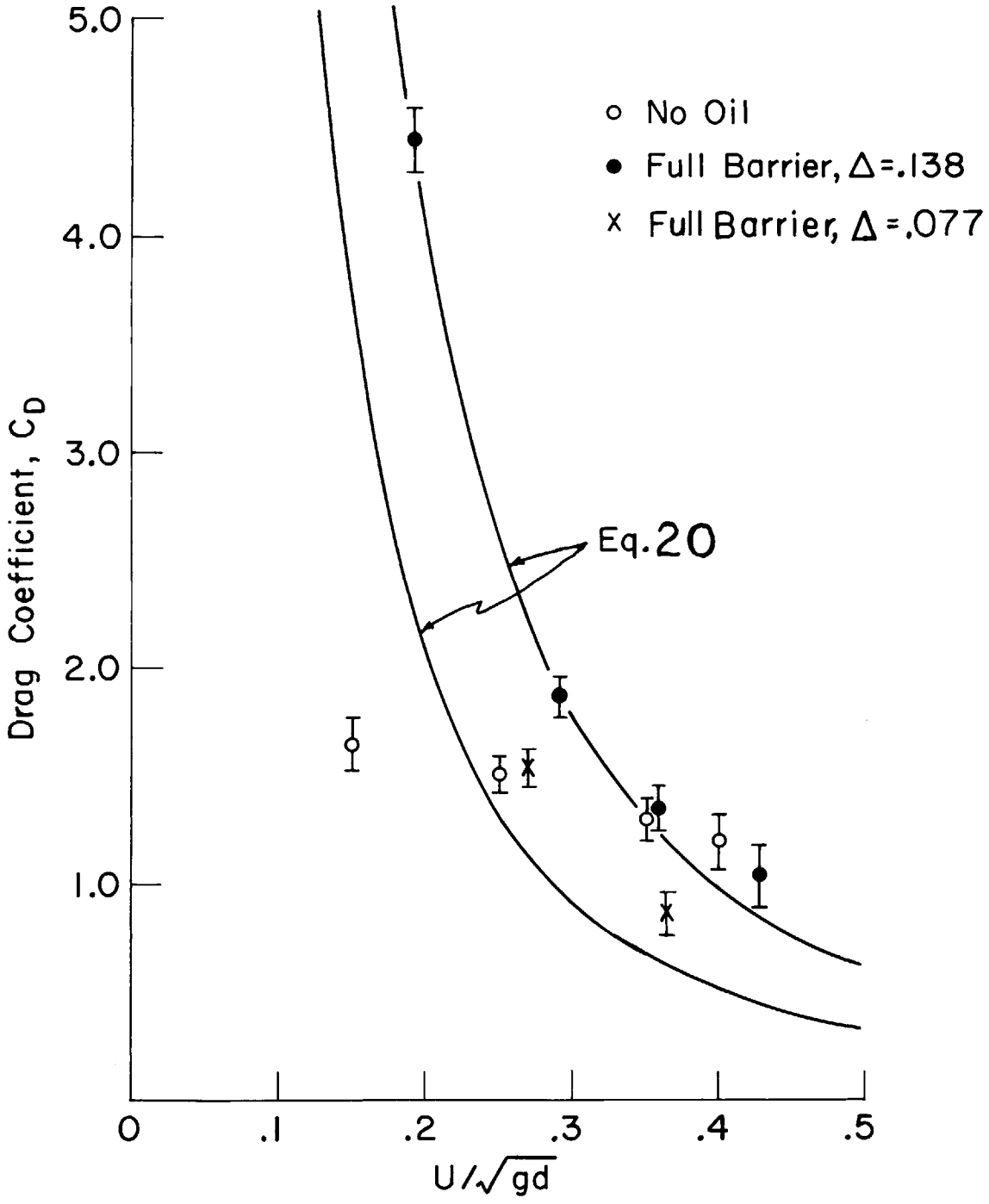

Figure 13. Drag coefficient, C_D, versus $U/\sqrt{gd}$

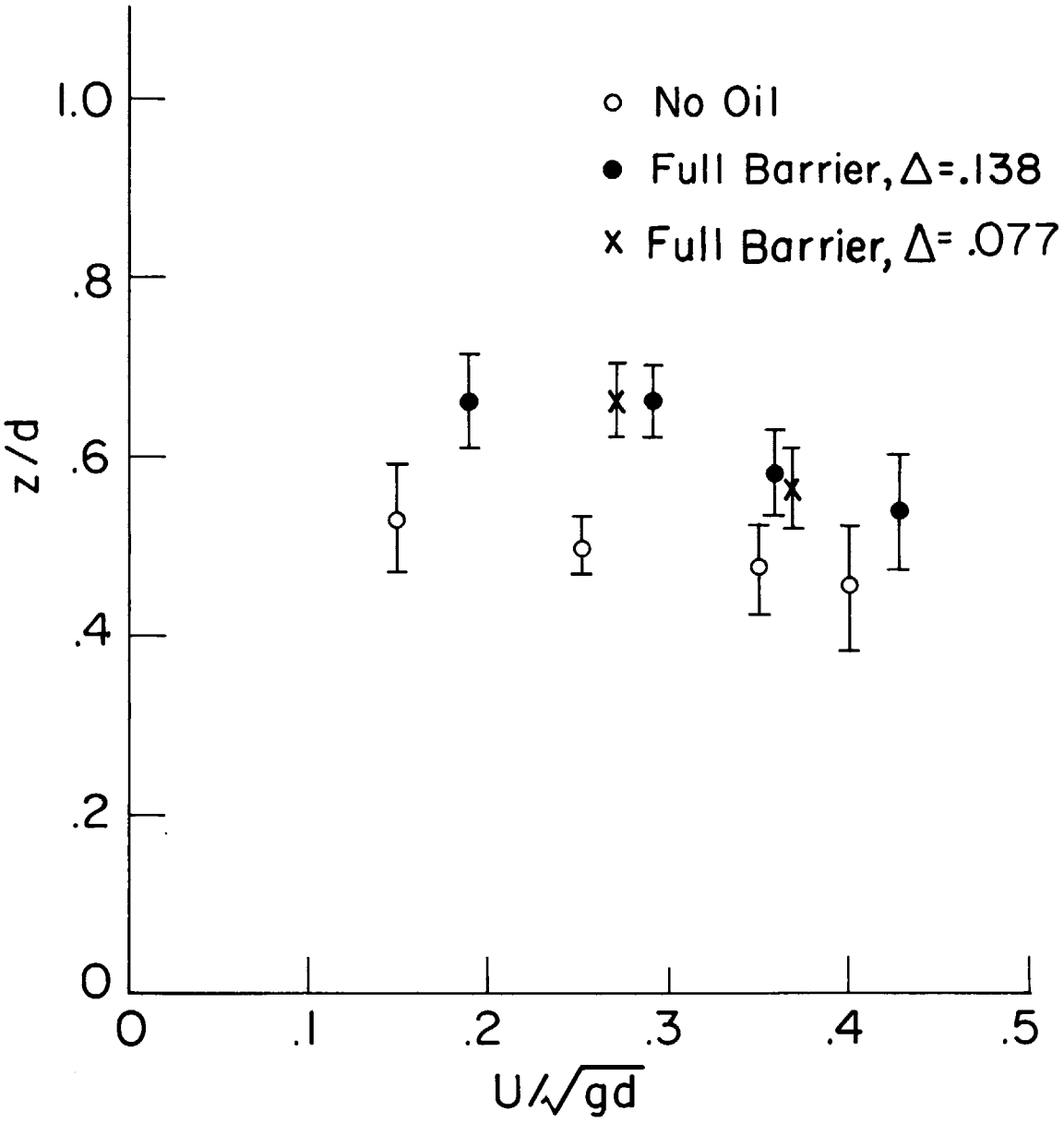

Figure 14. Location of drag force from lower edge of boom, z/d, versus $U/\sqrt{gd}$

would be a 10% shift in data at the full barrier end of the data.

The effects of different oils for full barriers drop out when C_D and z/d versus $(1 - \Delta)h/d$ are plotted for constant densimetric Froude number rather than just Froude number. For no oil, C_D and z/d depend on the Froude number, where the densimetric Froude number has no meaning. These effects can be seen in Figures 13 and 14.

The velocities in the oil are small; it could be expected that differences in oil motion for different oils (different viscosity) are negligible. No viscosity effects were noticed in the drag and moment measurements; all effects of different oils can be explained by differences in specific gravities.

It was shown in Section III.2 that when hydrostatic forces become large as compared with the dynamic forces, the hydrostatics give a good prediction of the drag and moment behavior (for large d/d_B, C_D, and z/d followed behavior predicted by hydrostatics). It is also reasonable to expect hydrostatics to play a role with oil present, since the velocities in the oil are small. Consider the situation where one side of the barrier is full of oil, thickness h, and the other side is water to a depth d, and there are negligible dynamic pressures. For a full barrier $(1 - \Delta)h/d = 1.0$, which implies that $h = \rho_w/\rho_0 d$. The force on the barrier per unit width is the difference in hydrostatic forces on each side as in equation (19).

$$D = \rho_0 g h^2/2 - \rho_w g d^2/2$$

$$D = (g d^2/2)(\rho_w/\rho_0 - 1)\rho_w \approx \rho_w g d^2 \Delta/2 \qquad (19)$$

The drag coefficient, assuming the velocity of the water under the barrier does not effect the hydrostatics, is given by equation (20),

$$C_D = D/\frac{1}{2}\rho_w dU^2 = \frac{gd}{U^2}(\rho_w/\rho_0 - 1)$$

$$C_D = \frac{1}{F^2}(\rho_w/\rho_0 - 1) \approx 1/F'^2 \qquad (20)$$

If the approximation is made that Δ, being $(\rho_w - \rho_0)/\rho_w$ is equal to $(\rho_w - \rho_0)/\rho_0$, then the approximation of equations (19) and (20) can be made. Equation (20) is plotted in Figure 13, C_D vs. Froude number for asymptotic d/d_B behavior, for both soybean oil and #2 fuel oil. The agreement with experimental results is quite close for low Froude number. For higher Froude numbers, when interfacial waves are present, agreement is only approximate.

The applied moment can be determined using hydrostatics. The center of hydrostatic force is 1/3 up from the lower edge; the difference in moments applied about the lower edge by the oil and water is given by equation (21).

$$M = \rho_0 g \frac{h^2}{2}\frac{h}{3} - \rho_w g \frac{d^2}{2}\frac{d}{3} = g\rho_w \frac{d^3}{6}\left(\frac{\rho_w^2 - \rho_0^2}{\rho_0^2}\right) \qquad (21)$$

The location of the drag force is given by M/D as in equation (22)

$$M/D = g\rho_w \frac{d^3}{6}\left(\frac{\rho_w^2 - \rho_0^2}{\rho_0^2}\right) \Big/ \frac{gd^2}{2}\rho_w\left(\frac{\rho_w}{\rho_0} - 1\right)$$

$$M/D = \frac{d}{3}\left(\frac{\rho_w + \rho_0}{\rho_0}\right) \approx \frac{2}{3}d \qquad (22)$$

If the term $((\rho_w + \rho_0)/\rho_0)$ is approximated by $2\rho/\rho$, then the location of drag is about 2/3 d from the lower edge. This 2/3 is in agreement with the results for low Froude number and approximately so for higher Froude number (see Figure 14).

The drag and moment results for the oil case scale as the Froude number and Δ; where Reynolds number (based on oil or water) effects are negligible.

IV. CONCLUSION, RESULTS APPLIED TO FULL SCALE

Oil spilled on the open sea can consist of anything from high grade fuel oil to crude oil with the more volatile fractions evaporated. If an oil spill is to be controlled by containment, an effective device must take into account how oil piles up against a barrier and what forces are exerted on the barrier by the action of water and oil. The results of this thesis answer some of the design questions involved with a boom containing oil in a steady current. The results also are part of the total situation when waves and wind are present.

The profile thickness of an oil slick held against a barrier normal to the current can be expected for the majority of its length to depend on the one-half power of the distance from the leading edge as in equation (23), where A is a constant dependent on the oil. Scale model results show that for soybean oil A = .090 and for #2 fuel oil A = .072.

$$h = \left(\frac{U^2}{g}\right)^{1/2} A x^{1/2} \tag{23}$$

Near the barrier and near the leading edge equation (23) only roughly applies. The error caused by neglecting these departures from the $x^{1/2}$ behavior have negligible effects when a boom holds large volumes. To determine maximum volumes held per unit width by a barrier, equation (23) can be integrated until h = d, as in equation (24). This result will apply as long as the densimetric Froude number is less than the critical Froude number; above the critical Froude number no oil will be held by the barrier.

$$V = d^2\left(\frac{2}{3}\right)\left(\frac{1}{A}\right)^2/F'^2 \tag{24}$$

Solving equation (23) for x and setting h = d gives an estimate of the slick length (for F' less than F'_{crit}) as in equation (25),

$$\ell = \left(\frac{g\Delta}{U^2}\right)\left(\frac{1}{A}\right)^2 d^2 = d\left(\frac{1}{A}\right)^2/F'^2 \tag{25}$$

Combining equations (24) and (25) gives the rule-of-thumb, $V = 2/3d\ell$, for barrier volumes given maximum thickness and slick length.

The operating chart for deployed booms should be Figure 8, dimensionless volume versus densimetric Froude number. A boom containing oil will have an operating point on the figure somewhere below the $1/F'^2$ law and to the left of the critical Froude number. Above the $1/F'^2$ line leakage occurs because the slick has become thicker than the boom draft; to the right of the critical Froude number leakage occurs because of the interfacial waves. Knowing any two of the three variables U, V, or d allows by use of the chart, the operating range of the third variable to be determined.

Barrier construction and strength is of prime concern in designing an effective barrier. From the results of measuring the drag coefficient for a flat plate, an estimate of the steady state tension on a stably deployed boom in a current can be expected to be given by equation (26), where L is the width of the boom in a direction perpendicular to the current, θ is the angle the barrier makes with the current at the mooring, and where no tangential forces are exerted by the flow. A deployed boom, moored at two ends against a current will

roughly follow a parabola.

$$T = (\frac{1}{2} \rho_w dLU^2 C_D)/\cos\theta \qquad (26)$$

The drag coefficient of equation (26) is given in Figure 13 and depends on the Froude number, Δ, and the volume of oil held by the barrier.

The location of the drag force depends on the operating conditions (Froude number and volume helds) and is given by Figure 14. When connection is made to a barrier it should be made somewhere around the center of the range of drag locations. This means connection is made between .45d and .67d from the lower edge, roughly somewhere above 50% of the draft. A barrier must have enough roll stability to withstand a moment per unit width of the drag force times the maximum shift in location of drag (around $\frac{2}{10}$ d), as in equation (27),

$$M_{roll} = (\frac{1}{2} \rho U^2 dC_D)(\frac{2}{10} d) \quad . \qquad (27)$$

The design criteria discussed in this section are results of a scale model study. Field observations of prototype situations are a necessary part of applying results to full scale. Once a range of field observations have been acquired (especially in terms of interfacial waves and critical Froude numbers), the results of this thesis will be able to be more readily applied to the design problem.

REFERENCES

1. Hoult, David P., 1970, "Containment of Oil Spills by Physical and Air Barriers", AIChE Meeting Presentation, San Juan, Puerto Rico, May 20, 1970.

2. Hoult, David P., 1969, "Containment and Collection Devices for Oil Slicks", p. 65 in Oil on the Sea (David P. Hoult, editor), Plenum Press, New York, New York.

3. Schlichting, Herman, 1960, Boundary Layer Theory, McGraw-Hill Book Company, Inc., New York, New York, p. 552.

4. ibid, p. 552.

5. Hunsakar, J. C., and Rightmire, B. G., 1947, Engineering Application of Fluid Mechanics, McGraw-Hill Book Company, Inc., New York, New York, pp 198-201.

6. ibid, p. 198.

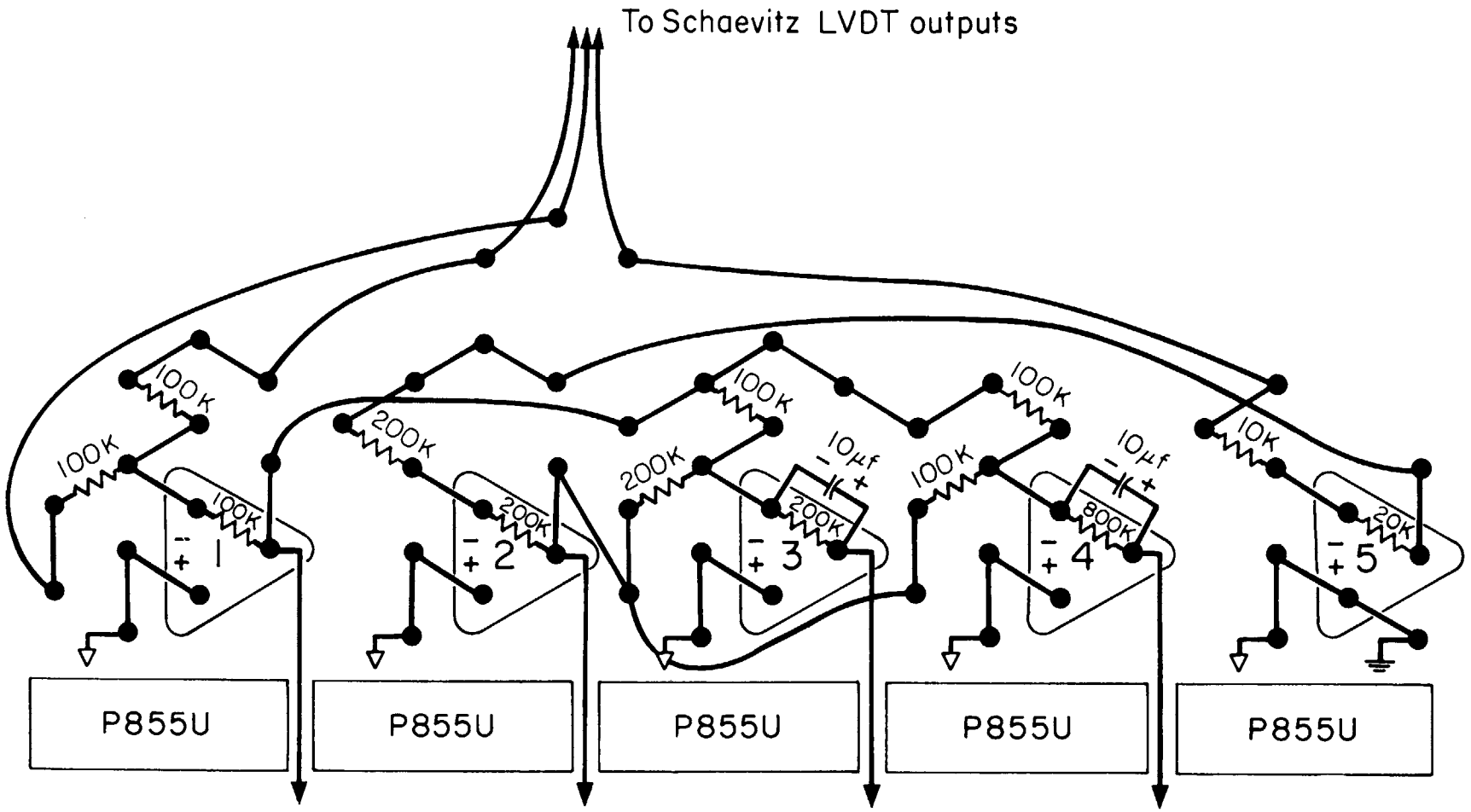

Appendix I. Philbrick-Nexus RP-4 operational manifold circuit program.